

# Simulation and Analysis of Co-phasing Errors of the Segmented Primary Mirror Tiled by Petal-shaped Segments in LOT\*

SHEN Shi-dong<sup>1,2,3</sup> CUI Xiang-qun<sup>1,2†</sup> ZHANG Yong<sup>1,2</sup>

(1 National Astronomical Observatories/Nanjing Institute of Astronomical Optics & Technology, Chinese Academy of Sciences, Nanjing 210042)

(2 CAS Key Laboratory of Astronomical Optics & Technology, Nanjing Institute of Astronomical Optics & Technology, Nanjing 210042)

(3 University of Chinese Academy of Sciences, Beijing 100049)

**ABSTRACT** In order to fulfill the requirement for astronomical observation in the optical-infrared band using large universal aperture optical telescopes, China is planning to construct a 12-meter large aperture optical-infrared telescope (LOT). LOT is of particular significance to Chinese astronomy and would be co-phased in the near-infrared waveband. The primary mirror of LOT will be constructed from either hexagonal segments or petal-shaped segments. Analysis of co-phasing errors using a segmented primary mirror tiled by petal-shaped segments for LOT has been presented. The proposed primary mirror of LOT has 72 petal-shaped segments and a 4.5-meter circular mirror in the center. Detailed theoretical derivation of co-phasing errors and simulation about out-plane errors separately and comprehensively have been provided. SR (Strehl Ratio) of LOT is greater than 0.8 when the RMS (Root Mean Square) value of normally distributed tip-tilt errors is less than  $0.016''$  or the RMS value of normally distributed piston error is less than 42.5 nm at the co-phasing wavelength  $1\ \mu\text{m}$ . The simulation results are of great importance for the segmented primary mirror with active optics in LOT.

**Key words** telescopes, methods: analytical, methods: data analysis, techniques: high angular resolution

**Classified index:** P111; **Document code:** A

## 1 Introduction

With the rapid development of astronomical science and technology, and the urgent need for large telescopes with higher light collecting capacity and resolution, many large aperture optical-

infrared telescopes have been built or are under construction both in China and abroad. The main approaches for the design of large aperture telescopes include: (1) the thin mirror active optics approach used in the VLT (Very Large Telescope) of the European Southern Observatory<sup>[1]</sup>; (2) the

Received 2021-12-16, revised version 2022-03-10

\*Supported by National Natural Science Foundation of China (NSFC) (Nos. U1931207, U2031207 and U1931126)

†xcui@niaot.ac.cn

segmented mirror active optics approach used in the KECK (Keck telescope) of the United States<sup>[2]</sup>; and (3) the combined thin mirror and segmented mirror active optics approach pioneered by LAMOST (Large Sky Area Multi-Object Fiber Spectroscopic Telescope) of China<sup>[3-5]</sup>. However, due to mirror size limitations, the current aperture limit of a single mirror is 8.4 m, which was successfully constructed by the Mirror Laboratory at University of Arizona. In order to construct larger or giant aperture telescopes, segmented mirror active optics has become the approach of choice taking into consideration factors such as technical difficulty, cost, and construction time.

To fulfill the requirements for astronomical observation in the optical-infrared band with large universal aperture optical telescopes, CFGT (Chinese Future Giant Telescope) was proposed in 2000, using a 30-meter primary mirror design with fan-shaped segments<sup>[6-11]</sup>. Japan subsequently proposed JELT (Japan Extremely Large Telescope), the primary mirror of which would also have been 30 m in size<sup>[12]</sup>. Japan has since built a middle aperture telescope, namely the Seimei telescope. The Seimei telescope is a 3.8-meter optical-infrared telescope, the primary mirror of which consists of 18 petal-shaped segments<sup>[13-14]</sup>.

Chinese astronomers proposed LOT (12-meter large aperture optical-infrared telescope) in 2016 and have considered the use of a segmented primary mirror<sup>[15-17]</sup>. However, there are two proposed segmentation schemes: one type is a segmented primary mirror tiled into 84 hexagonal segments which is commonly used in segmented mirror telescopes, and the other is an innovative design using a 4.5-meter circular center mirror and 72 petal-shaped segments. Fig. 1 depicts two types of segmentation schemes.

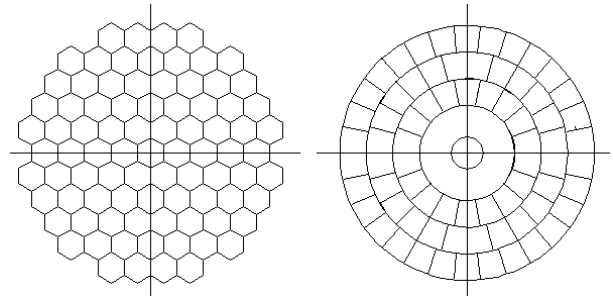


Fig. 1 Two types of segmentation schemes

The segmented primary mirror tiled into petal-shaped segments has numerous advantages compared to the segmented primary mirror tiled into hexagonal segments. For example, the primary mirror can have a circular profile, and the type of segments are consistent in every ring, regardless of physical size or profile. The number of petal-shaped segments required is also fewer than would be required using hexagonal segments for the same size of primary mirror, even though the area of an individual hexagonal segment and a petal-shaped segment is almost the same<sup>[18-20]</sup>. This paper will therefore focus on developing an innovative scheme as described in Table 1, in which the size parameters and quantity of each segment are introduced in detail. We can also consider adopting all fan-shaped segments for LOT. However, changing the inner 4.5-meter diameter to fan-shaped segments will not affect the research described in this paper from a practical point of view. Furthermore, a perfect co-phasing wavefront in visible imaging can be obtained by using this 4.5-meter mirror; thin mirror active optics technology can also be used in the central mirror to achieve a combination of thin mirror active optics and fan-shaped segmented mirror active optics if necessary.

The development of LOT is of great significance to Chinese astronomy, and the segmented mirror active optics approach is the preferred choice for LOT taking into consideration co-focus

in the visible band and co-phase in the infrared band<sup>[21–23]</sup>. Theoretical derivation and simulation of co-phasing errors are presented in this paper when the primary mirror of LOT reaches co-phase at  $1\ \mu\text{m}$ <sup>[24–27]</sup>.

**Table 1** The primary mirror of LOT tiled with fan-shaped segments

Ring number	Inner radius of ring/mm	Outer radius of ring/mm	Number of segments
first	775	2250	1
second	2250	3500	18
third	3500	4750	24
fourth	4750	6000	30

Error analysis and simulation are the prerequisites and necessary conditions for error allocation during the feasibility evaluation for any large aperture segmented telescope. Chanan et al.<sup>[28]</sup> got SR (Strehl Ratio) for KECK as a function of the RMS (Root Mean Square) segment co-phasing error. Besides, Troy et al.<sup>[29]</sup> analyzed the influence of gaps, secondary mirror obstruction and reflectivity of mirrors for TMT (Thirty Meter Telescope). In addition, Yaitskova et al.<sup>[30–32]</sup> derived the analytical expression for formulas describing highly segmented telescopes, established an optical calculation model of PSF (Point Spread Function) based on FFT (Fast Fourier Transform), and simulated the influence of piston and tip-tilt on SR of the telescope, providing data support for the construction of ELT (European Extremely Large Telescope).

In order to evaluate our proposed scheme and study the sensitivity of co-phasing errors, in this study we undertake theoretical derivation and simulation analysis of co-phasing errors in LOT in which the primary mirror is tiled by petal-shaped

segments. The results provide a reference and basis for the selection and construction of the primary mirror shape scheme of the LOT.

## 2 Analysis of co-phasing errors

Fig. 2 introduces the global coordinate system of the primary mirror and the local coordinate system of the segment. The  $XCY$  plane is the projection plane of the primary mirror in Fig. 2, and the  $Z$ -axis is the direction of the optical axis perpendicular to the  $XCY$  plane. Point  $C$  is the origin of the global coordinate system  $XYZ$ . The origin point,  $o$ , of the local coordinate system  $(xyz)$  of each segment is located at the center of circum-circle of the segment. The  $y$ -direction is the radial direction of the primary mirror and the  $z$ -direction is the normal direction of a segment, where  $x$  is perpendicular to  $y$  and  $z$ .

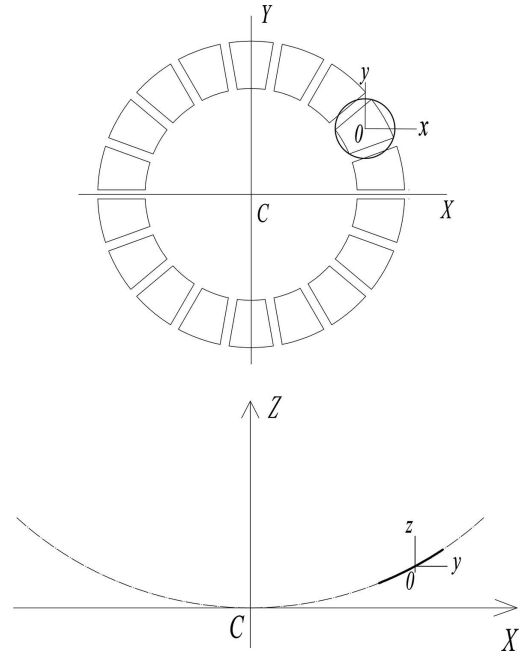


Fig. 2  $XCY$  plane in the primary mirror global coordinate system and  $yoZ$  plane in the segment local coordinate system

$W$  is assumed to be the wavefront of the primary mirror, and  $\Delta W$  is the wavefront error of the primary mirror.  $\omega_i$  is the wavefront of the  $i$ th segment, and  $(\Delta\omega)_i$  is the wavefront error of the  $i$ th segment. The formula to describe the approximate relationship between the Strehl Ratio and wavefront is as follows<sup>[33]</sup>:

$$\text{SR} = \exp \left[ - \left( \frac{2\pi}{\lambda} \sigma_{\text{wf}} \right)^2 \right], \quad (1)$$

where  $\sigma_{\text{wf}}$  is the RMS value of wavefront error (in wavelength units,  $\lambda$ ) in Eq. (1).

In addition,  $\sigma_{\text{wf}}$  can be expressed as<sup>[34]</sup>:

$$\sigma_{\text{wf}}^2 = \overline{(\Delta W)^2} - (\overline{\Delta W})^2, \quad (2)$$

where

$$\begin{cases} \overline{\Delta W} = \frac{\iint \Delta W \, dA}{\iint dA}, \\ \overline{(\Delta W)^2} = \frac{\iint (\Delta W)^2 \, dA}{\iint dA}. \end{cases} \quad (3)$$

Note that in Eq. (3),  $A$  represents the integral region of the primary mirror.

$$\iint \Delta W \, dA = \sum_{i=1}^N \iint (\Delta\omega)_i \, dz_i, \quad (4)$$

$$\iint (\Delta W)^2 \, dA = \sum_{i=1}^N \iint (\Delta\omega)_i^2 \, dz_i. \quad (5)$$

In Eq. (4) and Eq. (5),  $N$  represents the number of segments, and  $dz_i$  represents the integral region of the segment.

The radius of the circumcircle of a petal-shaped segment is  $a$ , the center of which is the center of its circumcircle. If the polar coordinate system  $(\rho, \theta)$  is considered with regard to the local coordinate system where  $\rho = r/a$ , the surface of

segment in the local coordinates can be expressed as a expansion<sup>[35]</sup>:

$$z(\rho, \theta) = \sum_{mn} \alpha_{mn} \rho^m \cos(n\theta), \quad (6)$$

$\alpha_{mn}$  is the local coordinate expansion coefficient, both  $m$  and  $n$  are integers and  $m \geq n \geq 0$  and  $m - n = \text{even}$  in Eq. (6).

The radius of curvature of the primary mirror,  $R_c$ , is  $-38400$  mm.  $p$  represents an off-axis distance from the center of a segment to the center of the primary mirror, and  $p = \sqrt{x_o^2 + y_o^2}$  (where  $x_o$  and  $y_o$  are the coordinates of point  $o$  in Fig. 2). The conic constant of the primary,  $k$ , has a value of  $-0.9837843$ .  $\alpha_{20}$  is the coefficient of the first term in Eq. (6), represents defocus. The coefficient of the second term in Eq. (6) that represents astigmatism,  $\alpha_{22}$ , is  $ka^2p^2/4R_c^3$ . The coefficient of the third term in Eq. (6), representing coma,  $\alpha_{31}$ , is  $ka^3p/2R_c^3$ . In this study, we primarily focus on the effects of astigmatism as this dominates in terms of wavefront aberrations<sup>[36]</sup>.

## 2.1 The influence of piston

If there is some random piston error  $\alpha_i$  which obeys normal distribution  $N(0, \sigma_\alpha^2)$  of the  $i$ th segment, the standard deviation  $\sigma_\alpha$  is the RMS value of piston error, we can obtain the wavefront of the  $i$ th segment:

$$(\omega)_i = 2\alpha_i. \quad (7)$$

The wavefront of the segmented primary mirror can also be obtained:

$$\begin{aligned} \overline{(\Delta W)^2} &= \frac{\iint (\Delta W)^2 \, dA}{\iint dA} \\ &= \frac{\sum_{i=1}^N \iint (\Delta\omega)_i^2 \, dz_i}{\sum_{i=1}^N \iint_{\text{seg}_i} dz_i} = 4\sigma_\alpha^2, \end{aligned} \quad (8)$$

$$\begin{aligned}
 (\overline{\Delta W})^2 &= \left( \frac{\iint \Delta W \, dA}{\iint dA} \right)^2 \\
 &= \left[ \frac{\sum_{i=1}^N \iint (\Delta\omega)_i \, dz_i}{\sum_{i=1}^N \iint_{\text{seg}_i} dz_i} \right]^2 = 0, \quad (9)
 \end{aligned}$$

where  $z_i$  represents the integral region of the  $i$ th segment and  $\text{seg}_i$  represents area of the  $i$ th segment. By substituting this result in Eq. (2), it can be concluded that:

$$\sigma_{\text{wf}}^2 = 4\sigma_\alpha^2. \quad (10)$$

At this time, the RMS value of piston error is  $0.0375\lambda$  when SR is 0.8 or  $\sigma_{\text{wf}}$  is  $0.075\lambda$ . The RMS value of piston should be less than 37.5 nm when the co-phasing wavelength is  $1 \mu\text{m}$ .

## 2.2 The influence of tip-tilt

We use the notation  $a_i$ ,  $\gamma_i$ ,  $\beta_i$  to represent the radius of circumcircle of the  $i$ th petal-shaped segment, the amount of tilt in the  $x$ -direction of the  $i$ th petal-shaped segment (in  $\lambda$  units), and the amount of tilt in the  $y$ -direction of the  $i$ th petal-shaped segment (in  $\lambda$  units) respectively. If  $\gamma_i \sim N(0, \sigma_\gamma^2)$  and  $\beta_i \sim N(0, \sigma_\beta^2)$ , the standard deviation  $\sigma_\gamma$  is the RMS value of tip and the standard deviation  $\sigma_\beta$  is the RMS value of tilt, the wavefront of the  $i$ th petal-shaped segment can be obtained:

$$\begin{aligned}
 (\Delta\omega)_i &= 2 \left( \frac{\gamma_i}{a_i} x + \frac{\beta_i}{a_i} y \right), \quad (11) \\
 \overline{(\Delta W)^2} &= \frac{\iint (\Delta W)^2 \, dA}{\iint dA}
 \end{aligned}$$

$$\begin{aligned}
 &= \frac{\sum_{i=1}^N \iint (\Delta\omega)_i^2 \, dz_i}{\sum_{i=1}^N \iint_{\text{seg}_i} dz_i} \\
 &= 0.58\sigma_\gamma^2 + 0.75\sigma_\beta^2, \quad (12)
 \end{aligned}$$

$$\begin{aligned}
 (\overline{\Delta W})^2 &= \left( \frac{\iint \Delta W \, dA}{\iint dA} \right)^2 \\
 &= \left[ \frac{\sum_{i=1}^N \iint (\Delta\omega)_i \, dz_i}{\sum_{i=1}^N \iint_{\text{seg}_i} dz_i} \right]^2 = 0. \quad (13)
 \end{aligned}$$

Assuming that the standard deviation of the normal distribution of tip-tilt is the same, we can conclude that:

$$\sigma_{\text{wf}}^2 = 1.3298\sigma^2. \quad (14)$$

The RMS value of tip-tilt error  $\sigma$  is  $0.065\lambda$  when SR is 0.8 or  $\sigma_{\text{wf}}$  is  $0.075\lambda$ . The RMS value of tip-tilt error should be less than  $0.016''$  ( $\sigma_{\text{wf}}/a_i$ ) when the co-phasing wavelength is  $1 \mu\text{m}$ . The theoretical co-phasing errors of the two segmented mirror schemes using hexagonal segments<sup>[37]</sup> and petal-shaped segments are compared in Table 2.

**Table 2 Comparison of RMS value of co-phasing errors between two segment shapes**

	Primary mirror tiled by hexagonal segments	Primary mirror tiled by petal-shaped segments
Co-phasing error		
Piston/nm	37.8	37.5
Tip-tilt/''	0.017	0.016

### 2.3 The influence of in-plane errors

Decenter in  $x$  axis can be ignored among the three in-plane errors, based on the rotational symmetry of the quadric surface. Here, the radial error decenter in  $y$  axis and clocking error are mainly analyzed. We assume that the radial error of radial distance  $p$  of the  $i$ th fan-shaped segment can be expressed as  $(\Delta p)_i$  (in  $\lambda$  units), and  $(\Delta p)_i \sim N(0, \sigma_{\Delta p}^2)$ ,  $\sigma_{\Delta p}$  is the RMS value of radial translation error. The radial distance of fan-shaped segments in the first ring is  $p_1$ , with a value of 2.919352 m. The radial distance of fan-shaped segments in the second ring is  $p_2$ , 4.160594 m and the radial distance of fan-shaped segments in the third ring is  $p_3$ , 5.404607 m, then it can be calculated as follows:

$$\begin{aligned} \overline{(\Delta W)^2} &= \frac{\sum_{i=1}^N \iint (\Delta \omega)_i^2 dz_i}{\sum_{i=1}^N \iint_{\text{seg}_i} dz_i} \\ &= \left( \frac{ka^2}{R_c^3} \right)^2 \frac{\sum_{i=1}^N \iint p_i^2 (\Delta p)_i^2 \rho^4 \cos^2(2\theta) dz_i}{\sum_{i=1}^N \iint_{\text{seg}_i} dz_i} \\ &= 1.48106 \times 10^{-10} \sigma_{\Delta p}^2, \end{aligned} \quad (15)$$

$$\begin{aligned} \overline{(\Delta W)}^2 &= \left[ \frac{\sum_{i=1}^N \iint (\Delta \omega)_i dz_i}{\sum_{i=1}^N \iint_{\text{seg}_i} dz_i} \right]^2 \\ &= \left( \frac{ka^2}{R_c^3} \right)^2 \left[ \frac{\sum_{i=1}^N \iint p_i (\Delta p)_i \rho^2 \cos(2\theta) dz_i}{\sum_{i=1}^N \iint_{\text{seg}_i} dz_i} \right]^2 \\ &= 0, \end{aligned} \quad (16)$$

$$\sigma_{\text{wf}}^2 = 1.48106 \times 10^{-10} \sigma_{\Delta p}^2, \quad (17)$$

where  $p_i$  is the radial distance of the  $i$ th segment.

In this case, the  $\sigma_{\text{wf}}$  value is  $0.075\lambda$  when SR is 0.8. The RMS value of radial translation error  $\sigma_{\Delta p}$  is 6162.8 $\lambda$ . The RMS value of radial translation error of each fan-shaped segment should be less than 6.162 mm when the co-phasing wavelength is 1  $\mu\text{m}$ .

Assuming that the clocking error of the  $i$ th fan-shaped segment can be expressed as  $(\Delta \theta)_i$  (radian units), and  $(\Delta \theta)_i \sim N(0, \sigma_{\Delta \theta}^2)$ , the wavefront error of the  $i$ th fan-shaped segment can be obtained:

$$(\Delta \omega)_i = 2 \frac{\partial z_i}{\partial \theta_i} (\Delta \theta)_i = 2 \frac{kp_i^2}{R_c^3} xy (\Delta \theta)_i, \quad (18)$$

$$\begin{aligned} \overline{(\Delta W)^2} &= \frac{\sum_{i=1}^N \iint (\Delta \omega)_i^2 dz_i}{\sum_{i=1}^N \iint_{\text{seg}_i} dz_i} \\ &= \left( \frac{k}{R_c^3} \right)^2 \frac{\sum_{i=1}^N \iint p_i^4 (\Delta \theta)_i^2 4x^2 y^2 dz_i}{\sum_{i=1}^N \iint_{\text{seg}_i} dz_i} \\ &= 7.758 \times 10^{-9} \sigma_{\Delta \theta}^2, \end{aligned} \quad (19)$$

$$\begin{aligned} \overline{(\Delta W)}^2 &= \left[ \frac{\sum_{i=1}^N \iint (\Delta \omega)_i dz_i}{\sum_{i=1}^N \iint_{\text{seg}_i} dz_i} \right]^2 \\ &= \left( \frac{k}{R_c^3} \right)^2 \left[ \frac{\sum_{i=1}^N \iint p_i^2 (\Delta \theta)_i 2xy dz_i}{\sum_{i=1}^N \iint_{\text{seg}_i} dz_i} \right]^2 \\ &= 0, \end{aligned} \quad (20)$$

$$\sigma_{\text{wf}}^2 = 7.758 \times 10^{-9} \sigma_{\Delta\theta}^2. \quad (21)$$

In this case, the  $\sigma_{\text{wf}}$  value is  $0.075\lambda$  when SR is 0.8. The RMS value of radial translation error  $\sigma_{\Delta\theta}$  is  $2.93'$  when the co-phasing wavelength is  $1 \mu\text{m}$ .

### 3 Simulation results of co-phasing errors

As described above, a number of approximate

calculations are required in the theoretical derivation of the co-phasing errors of the primary mirror which need to be implemented in the simulation software. The LOT model was established to simulate real co-phasing errors, which were used for the final reference and comparative verification of the simulation analysis. Nasmyth focal system of LOT will be built as a priority in order to meet the requirements of domestic astronomers for fine detail observation. The parameters are shown in Table 3.

**Table 3** Main parameters of Nasmyth focal system of LOT (Focal ratio F number/14.4)

Surface position	Curvature radius /mm	Thickness /mm	Diameter /mm	Aspheric coefficient
primary mirror	-38400	-16318.562	12447	Quadratic: -0.9837843
secondary mirror	-7680.99	22268.562	1811	Quadratic: -2.5518687 Sixth degree: $-6.39323 \times 10^{-23}$

Fig. 3 is a ring of petal-shaped segments in the aperture. The inner radius and outer radius of a segment are given by  $r$ ,  $R$  respectively and the space between adjacent segments is  $2d$  in Fig. 3. A1 and B1 represent two vertices of a segment respectively.

The four vertices of a segment are calculated, and a program was written to generate the segment aperture, which would then be imported into ZEMAX software for the next stage of the simulation.

The fan-shaped segments in each ring can be solved by calculating values for one of the fan-shaped segments in a given position, and then rotated to obtain the positions of the other segments in the same ring. For example, the coordinates A1 and B1 of a segment in the second ring are calculated according to

$$\begin{cases} \delta_1 = \arcsin \frac{d}{R} \\ \alpha = 20^\circ - \delta_1 \\ x_{A1} = R \cos \delta_1 \\ y_{A1} = -R \sin \delta_1 \end{cases}, \quad (22)$$

and

$$\begin{cases} \delta_2 = \arcsin \frac{d}{r} \\ \beta = 20^\circ - \delta_2 \\ x_{B1} = R \cos(20^\circ - \delta_2) \\ y_{B1} = -R \sin(20^\circ - \delta_2) \end{cases}. \quad (23)$$

The segment aperture program is used to generate the corresponding aperture, which would be imported into ZEMAX software for the next simulation.

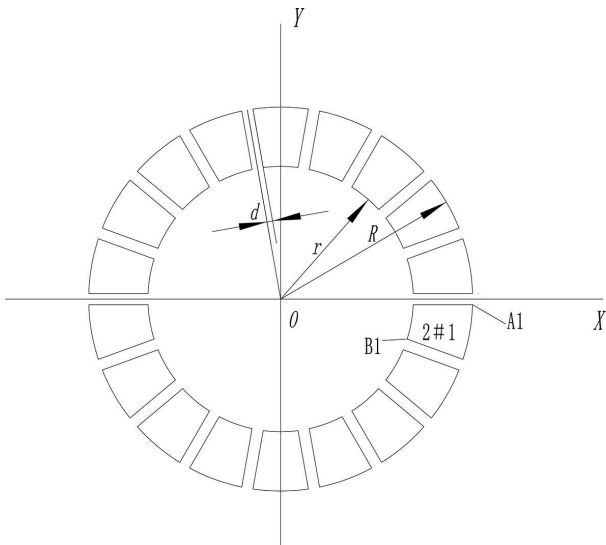


Fig. 3 Diagram of calculating the aperture of petal-shaped segment

The loss of light-gathering energy is 0.41% which is very small compared to the light loss caused by the secondary mirror and the central hole of the M4 mirror in LOT, assuming the space between the fan-shaped segments is 3 mm. It is further calculated that the energy loss values are 1.3% and 2.6% when the gap between fan-shaped segments is 10 mm and 20 mm, respectively. The SR value of LOT is 1 in both cases, and it can therefore be concluded that the gap between the segments has no effect on the image quality except for the shadow effect on the final diffraction pattern.

Each petal-shaped segment has six degrees of freedom and different reflective surface properties, and all segments are independent in the non-sequence mode of ZEMAX software. This method can simulate the actual segmented mirror system as shown in Fig. 4. Since three in-plane degrees of freedom of a segment, such as radial displacement and rotation about the center of a segment, can be guaranteed by the machining accuracy, the influence of the three out-of-plane degrees of freedom

will be mainly simulated.

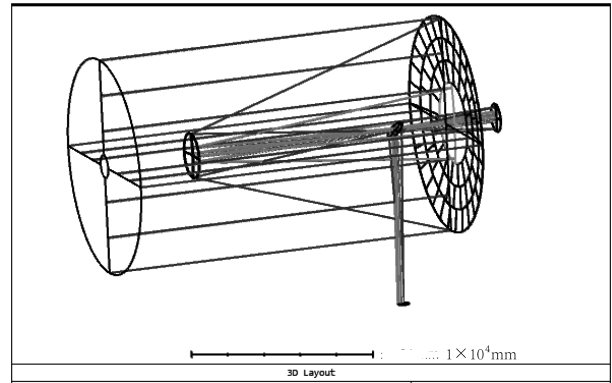


Fig. 4 3D layout of LOT

### 3.1 Comprehensive simulation analysis of tip-tilt

The Monte Carlo method is used to analyze the sensitivity of tip-tilt errors. The tilt angles of 72 segments in ZEMAX software obey the same normal distribution. The tolerance width is  $\pm 2\sigma$  (where  $\sigma$  is the standard deviation), where the two ends of the width are equal to the maximum and minimum values of the tolerance operands, and RMS of tilt angles is  $\sigma$  if wavefront error RMS is used as the error evaluation standard. If the tilt angles of all segments are uniformly distributed, the tolerance width is  $\pm\nu$ , and both ends of the width are equal to the maximum and minimum values of the tolerance operands, the RMS value of tilt angles is given by  $\nu/\sqrt{3}$ .

Firstly, a comprehensive simulation analysis of tip-tilt is carried out. It is assumed that the two types of errors obey the same normal distribution with a tolerance range of  $\pm 0.032''$ . The simulation results are shown in Table 4, and the wavefront of the primary mirror is better than  $0.0755\lambda$  ( $\lambda$  is  $1\ \mu\text{m}$ ) for 90% of the processes. The calculated SR of telescope will be larger than 0.8 when the tip-tilt RMS value is less than  $0.016''$ , which is consistent with the theoretically derived value. A

simulation result is shown in Fig. 5, in which the RMS value of tip-tilt is  $0.015''$ , the RMS value of the wavefront of LOT is  $0.068\lambda$  ( $\lambda$  is  $1\ \mu\text{m}$ ) and the SR value of LOT is 0.84.

**Table 4 Simulation results of the influence of tip-tilt on SR (subject to normal distribution)**

Process	Wavefront of the primary mirror/ $\lambda$
98%	$< 0.08166429$
90%	$< 0.07552163$
80%	$< 0.07222136$
50%	$< 0.06577899$
20%	$< 0.05978577$
10%	$< 0.05628555$
2%	$< 0.05126353$

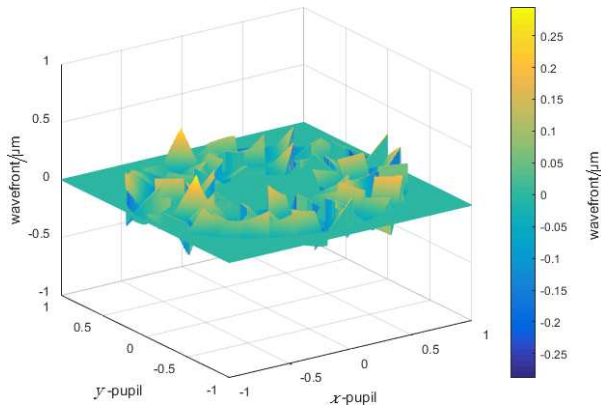


Fig. 5 Wavefront of LOT (RMS value of tip-tilt is  $0.015''$ )

In addition, it is assumed that tip-tilt is uniformly distributed at the same time and the tolerance range is  $\pm 0.025''$ . The simulation results are as follows in Table 5.

The simulation results show that the wavefront of the telescope in 90% of the processes is better than  $0.0758\lambda$ , indicating that the SR value

of the telescope is greater than 0.8 when the RMS value of the uniformly distributed tip-tilt errors is less than  $0.0145''$ . One of the simulation results is shown in Fig. 6, where the RMS value of tip-tilt is  $0.013''$ , the RMS value of the wavefront of LOT is  $0.0588\lambda$  (co-phasing wavelength  $\lambda$  is  $1\ \mu\text{m}$ ) and the SR of LOT is 0.847.

**Table 5 Simulation results of the influence of tip-tilt on SR (subject to uniform distribution)**

Process	Wavefront of the primary mirror/ $\lambda$
98%	$< 0.08057038$
90%	$< 0.07583863$
80%	$< 0.07328291$
50%	$< 0.06786719$
20%	$< 0.062254567$
10%	$< 0.05917826$
2%	$< 0.05351857$

### 3.2 Simulation analysis of piston

Monte Carlo analysis for the piston of all segments is undertaken, as the piston of each segment can be assumed to follow a normal distribution. The average value of piston is 0, and the tolerance range is  $\pm 85\ \text{nm}$ . 90% of processes will be better than  $0.075\lambda$  ( $\lambda$  is  $1\ \mu\text{m}$ ), which is taken as the evaluation criterion, and simulation results are shown in Table 6. The RMS value of the wavefront of the telescope in 90% of the processes is less than  $0.072\lambda$ , indicating that the SR of telescope is greater than 0.8 when RMS of piston is less than  $42.5\ \text{nm}$ . One of the simulation results is shown in Fig. 7, in which the RMS value of piston is  $30.5\ \text{nm}$ , the RMS value of the wavefront of LOT is  $0.0596\lambda$  (co-phasing wavelength  $\lambda$  is  $1\ \mu\text{m}$ ) and the SR of LOT is 0.87.

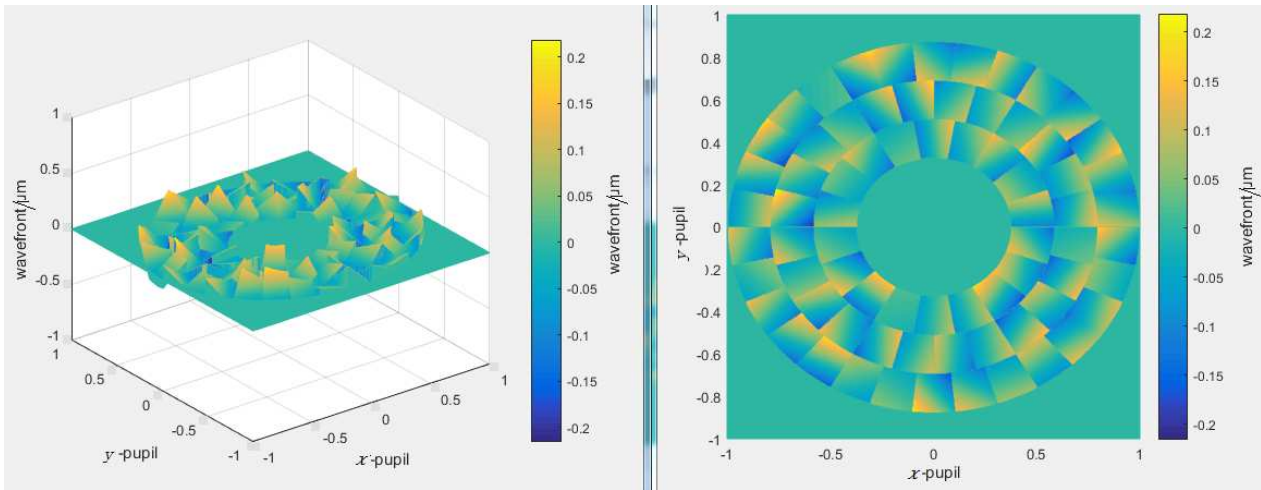


Fig. 6 Wavefront of LOT in a simulation of uniformly distributed tip-tilt (RMS value of tip-tilt is  $0.013''$ )

**Table 6 Simulation results of the influence of piston on SR (subject to normal distribution)**

Process	Wavefront of the primary mirror/ $\lambda$
98%	$< 0.07893314$
90%	$< 0.07153808$
80%	$< 0.06696024$
50%	$< 0.06033449$
20%	$< 0.05386300$
10%	$< 0.05034328$
2%	$< 0.04437901$

In addition, the simulation results indicate the RMS value of the wavefront in 90% of processes in Monte Carlo analysis is superior to  $0.075\lambda$ , assuming that piston of segments are uniformly distributed with a tolerance range of  $\pm 71$  nm. Simulation results are shown in Table 7. The SR of the telescope is greater than 0.8 when the RMS value of uniformly distributed piston is less than 41 nm. One of the results of the simulation is shown in Fig. 8, in which the RMS value of piston is 36.1 nm, the RMS value of the wavefront of LOT is  $0.07\lambda$  (co-

phasing wavelength  $\lambda$  is  $1 \mu\text{m}$ ) and the SR of LOT is 0.822.

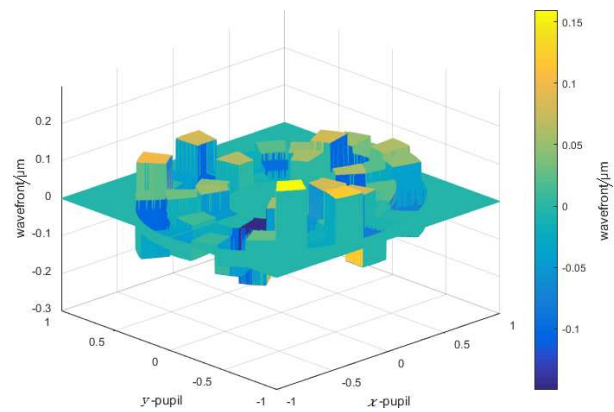


Fig. 7 Wavefront of LOT (RMS value of piston is 30.5 nm)

### 3.3 Comprehensive simulation analysis of tip-tilt and piston

Table 8 shows theoretical values of tip-tilt and piston that are normally distributed with the same weighting. Monte Carlo analysis of the out-of-plane errors is presented below, aiming for 90% of the simulation processes to be better than  $0.075\lambda$

( $\lambda$  is  $1 \mu\text{m}$ ). The piston of all segments is normally distributed and has a range of  $\pm 56 \text{ nm}$  and an average value of 0. In addition, tip-tilt values of all segments follow a normal distribution, with a range of  $\pm 0.024''$  and an average value of 0. The simulation results are shown in Table 9.

$0.012''$  and the RMS value of piston is less than  $28 \text{ nm}$ . The RMS value of the wavefront of the telescope is  $0.06125\lambda$  and  $\text{SR} = 0.867$ , given one of the integrated simulation processes, seen in Fig. 9, where the RMS value of tip-tilt is  $0.009''$  and the RMS value of piston is  $23.4 \text{ nm}$ .

**Table 7 Simulation results of the influence of piston on SR (subject to uniform distribution)**

Process	Wavefront of the primary mirror/ $\lambda$
98%	$< 0.08112048$
90%	$< 0.07536002$
80%	$< 0.07229380$
50%	$< 0.06577642$
20%	$< 0.05916804$
10%	$< 0.05554281$
2%	$< 0.05149642$

**Table 8 Theoretical values of tip-tilt and piston with equal weighting effect**

Theoretical SR of the primary mirror	Theoretical RMS of tip-tilt/ $''$	Theoretical RMS of piston/nm
0.64	0.016	37.5
0.73	0.014	32
0.78	0.012	28
0.8	0.011	26.5
0.87	0.009	21

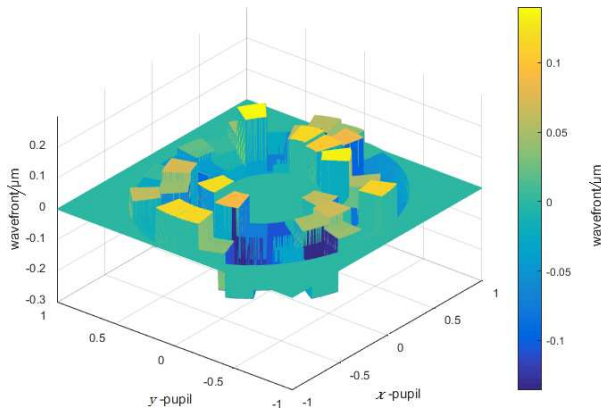


Fig. 8 Wavefront of LOT (RMS value of piston is  $36.1 \text{ nm}$ )

**Table 9 Simulation results of out-of-plane errors (subject to normal distribution, equal weight)**

Process	Wavefront of the primary mirror/ $\lambda$
98%	$< 0.07871465$
90%	$< 0.07239059$
80%	$< 0.06899876$
50%	$< 0.06320540$
20%	$< 0.05746286$
10%	$< 0.05447954$
2%	$< 0.04920690$

The simulation results show that the RMS value of the wavefront for 90% of processes is better than  $0.07235\lambda$ . Therefore, the SR of the telescope is greater than 0.8 when the RMS value of tip-tilt with a normal distribution is less than

The requirement for the tip-tilt error of segments can be relaxed and the RMS value of piston can be reduced to  $20 \text{ nm}$  or  $15 \text{ nm}$  in practical engineering. The comprehensive simulation results are

shown in Table 10 and Table 11.

RMS of the wavefront of LOT is better than  $0.074\lambda$  during 90% of the processes in Table 10, indicating that the SR of the telescope is better than 0.8 when the RMS value of piston is less than 20 nm and the RMS value of tip-tilt is less than  $0.014''$ . The RMS of the wavefront of LOT is better than  $0.0746\lambda$  during 90% of the processes in Table 11, indicating that the SR of the telescope is greater than 0.8 when the RMS of piston is less than 15 nm and the RMS of tip-tilt is less than  $0.015''$ .

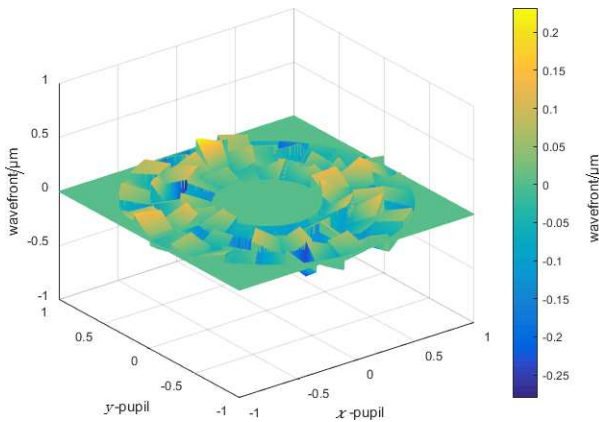


Fig. 9 Wavefront of LOT (RMS value of tip-tilt is  $0.009''$  and RMS value of piston is 23.4 nm).

**Table 10 Monte Carlo simulation results of out-of-plane errors (RMS value of piston is 20 nm and RMS value of tip-tilt is  $0.014''$ )**

Process	Wavefront of the primary mirror/ $\lambda$
98%	< 0.08010569
90%	< 0.07394273
80%	< 0.07052091
50%	< 0.06431928
20%	< 0.05843499
10%	< 0.05552909
2%	< 0.05009355

**Table 11 Monte Carlo simulation results of out-of-plane errors (RMS value of piston is 15 nm and RMS value of tip-tilt is  $0.015''$ )**

Process	Wavefront of the primary mirror/ $\lambda$
98%	< 0.08043108
90%	< 0.07465036
80%	< 0.07154468
50%	< 0.06524156
20%	< 0.05896498
10%	< 0.05576923
2%	< 0.05011820

## 4 Conclusion

The Chinese optical infrared astronomy community has strong potential to develop into an international-class community; however, it is challenging to grow this potential without a large telescope like LOT as a platform. Therefore, there is a strong need of a general-purpose optical telescope for China, which could be equipped with different scientific instruments.

We study tiling schemes using fan-shaped segments, and consider the influence of various tiling errors from the segmented primary mirror on image quality, especially the Strehl Ratio, and complete the theoretical derivation for the whole segmented mirror active optics simulation procedure. The segment errors, including three out-plane segment errors, are simulated using both numerical and synthetic approaches, with a lot of simulation results successfully achieved. The SR of LOT is greater than 0.8 when the RMS value of normally distributed tip-tilt errors is less than  $0.016''$  or the RMS value of normally distributed piston error is less than 42.5 nm with the co-phasing wavelength  $1\ \mu\text{m}$ . The comprehensive simulation analysis of the three out-of-plane errors shows that the

RMS value of tip-tilt should be less than  $0.012''$  and the RMS value of piston should be less than 28 nm when tip-tilt and piston are normally distributed with the same weighting. In addition, the RMS value of normally distributed tip-tilt should be less than  $0.014''$  when the RMS value of normally distributed piston is 20 nm. The RMS value of normally distributed tip-tilt should be less than  $0.015''$  when the RMS value of normally distributed piston is 15 nm.

The fan-shaped segmented mirror scheme is similar to the hexagonal segmented mirror scheme in terms of co-phasing errors, but the fan-shaped segmented mirror scheme is a better choice based on the processing cost and time. The results can be used as a reference for LOT and will provide LOT with the right to choose the scheme. Our results have important implications for the future development of large diameter optical-infrared telescopes.

### References

- [1] Merkle F, Hubin N. SPIE, 1991, 1542: 283
- [2] Nelson J E, Gillingham P R. SPIE, 1994, 2199: 82
- [3] Wang S G, Su D Q, Chu Y Q, et al. ApOpt, 1996, 35: 5155
- [4] Su D Q, Wang Y N. AcApS, 1997, 17: 315
- [5] Su D Q, Cui X Q, Wang Y N, et al. SPIE, 1998, 3352: 76
- [6] Su D Q, Cui X Q, Wang Y N, et al. SPIE, 2000, 4004: 340
- [7] Cui X Q, Su D Q, Wang Y N. IAU Joint Discussion, 2003, 25: E53
- [8] Xu X Q, Yan C H. SPIE, 2004, 5489: 1210
- [9] Li X N, Cui X Q, Guo W Y, et al. SPIE, 2004, 5494: 329
- [10] Li G P, Yang D H. SPIE, 2004, 5495: 204
- [11] Jiang L Y, Li X N. SPIE, 2010, 7656: 76566H
- [12] Iye M, Wg J. SPIE, 2004, 5489: 417
- [13] Shimono A, Iwamuro F, Kurita M, et al. SPIE, 2012, 8444: 84445Z
- [14] Kurita M, Kino M, Iwamuro F, et al. PASJ, 2020, 72: 48
- [15] Cui X Q, Zhu Y T. SPIE, 2016, 9906: 990607
- [16] Su D Q, Liang M, Yuan X Y, et al. MNRAS, 2016, 460: 2286
- [17] Su D Q, Liang M, Yuan X Y, et al. MNRAS, 2017, 469: 3792
- [18] Xiao G H, Guo W Y, Li X N. AR&T, 2004, 1: 289
- [19] Sun S X, Wang G M. AR&T, 2008, 5: 176
- [20] Song J B, Li G P. AR&T, 2010, 7: 355
- [21] Su D Q, Cui X Q. PrA, 1999, 17: 1
- [22] Su D Q, Zou W Y, Zhang Z C, et al. SPIE, 2000, 4003: 417
- [23] Su D Q, Cui X Q. ChJAA, 2004, 4: 1
- [24] Chanan G, Troy M, Dekens F, et al. ApOpt, 1998, 37: 140
- [25] Chanan G, Ohara C, Troy M. ApOpt, 2000, 39: 4706
- [26] Zhang Y, Wang Q M, Li Y P, et al. SPIE, 2014, 9145: 91454Y
- [27] Zhang Y, Cui X Q, Li H M, et al. SPIE, 2014, 9145: 91454W
- [28] Chanan G, Troy M. ApOpt, 1999, 38: 6642
- [29] Troy M, Chanan G. ApOpt, 2003, 42: 3745
- [30] Yaitskova N, Dohlen K. SPIE, 2000, 4003: 279
- [31] Yaitskova N, Dohlen K. JOSAA, 2002, 19: 1274
- [32] Yaitskova N, Dohlen K, Dierickx P. JOSAA, 2003, 20: 1563
- [33] Pan F Y, Burge J H, Zehnder R, et al. ApOpt, 2004, 43: 2632
- [34] Baiocchi D, Burge J H. SPIE, 2000, 4093: 58
- [35] Nelson J E, Mast T S, Faber S M. The Design of the Keck Observatory and Telescope: Keck Observatory Report 90. Caltech, 1985: 1
- [36] Nelson J E, Gabor G, Hunt L K, et al. ApOpt, 1980, 19: 2341
- [37] Shen S D, Cui X Q, Zhang Y. RAA, 2021, 21: 245

# 基于扇形子镜的12 m光学红外望远镜拼接共相误差仿真分析

沈世东<sup>1,2,3</sup> 崔向群<sup>1,2</sup> 张 勇<sup>1,2</sup>

(1 中国科学院国家天文台南京天文光学技术研究所 南京 210042)

(2 中国科学院天文光学技术重点实验室 南京 210042)

(3 中国科学院大学 北京 100049)

**摘要** 为满足国内对应用大型通用光学望远镜在光学红外波段进行天文观测的需求,中国规划建设一架12 m大口径光学红外望远镜(12-meter large aperture optical-infrared telescope, LOT). LOT对于中国天文界具有极其重要的意义,将会在近红外波段实现共相. LOT的主镜将采用子镜拼接的方案,由72块扇形子镜拼接而成,并且中央部分有一块直径4.5 m的圆形镜. 分析了采用扇形子镜拼接方案下LOT的共相误差,提供了详细的共相误差理论推导过程,并对包括3种子镜面外误差在内的误差源进行深入的单独模拟和综合模拟. 在共相波长为1  $\mu\text{m}$ 的条件下,当服从正态分布的倾斜误差的均方根值小于0.016"或服从正态分布的活塞误差的均方根值小于42.5 nm时, LOT的斯特列尔比大于0.8. 仿真结果对于采用共相拼接镜面主动光学的主镜在LOT中的应用具有重要意义.

**关键词** 望远镜, 方法: 分析, 方法: 数据分析, 技术: 高角分辨率